JOURNAL OF MATERIALS SCIENCE 26 (1991) 5566–5574

Electron microscope study of non-stoichiometric titania

M. REECE, R. MORRELL
Division of Materials Metrology, National Physical Laboratory, Teddington, Middlesex, TW11 0LW, UK

The distribution and coexistence of Magnéli phases (Ti_nO_{2n-1}) with $n = 4$, 5 and 6 in hydrogen-reduced TiO_2 has been investigated using transmission electron microscopy. The major phase was Ti_5O_9. Ti_6O_{11} was found in Ti_5O_9 grains in the form of narrow lamellae (<10 nm wide) epitaxially intergrown on (0 0 1) planes. The Ti_4O_7 phase, however, was never observed as a second phase in Ti_5O_9 grains but formed single-phase grains. The Ti_5O_9 phase was twinned on the $(0\,1\,1)_r$ planes of the rutile subcell structure and the Ti_6O_{11} lamellae were pinned to these twins. This pinning may be responsible for the hysteresis that occurs during the oxidation–reduction of non-stoichiometric TiO_2. We also report observations on *in situ* oxidation of the line phases.

1. Introduction

The mechanisms by which oxides are able to accommodate deviations from stoichiometry have been of interest to solid state physicists for some years [1–6], and great advances in the understanding of these mechanisms have been achieved by using transmission electron microscopy (TEM), particularly using lattice imaging and electron diffraction techniques [7–14]. The physical properties of non-stoichiometric oxides are strongly influenced by their exact composition, and for this reason they represent a class of materials with interesting and novel properties that are put to use in, for example, zirconia oxygen sensors and high-T_c superconductors.

There are several mechanisms by which oxides can accommodate non-stoichiometry to form stable phases. At small deviations from stoichiometry the low density of point defects produced are distributed randomly, but as their concentration increases their interaction also increases and they can become ordered. This ordering can take the form of defect clusters, as is the case for oxygen excess wustite ($Fe_{1-x}O$); long-range ordering of the point defects to produce superstructures; or the formation of crystallographic shear structures, which have been studied extensively in rutile (TiO_2), molybdenum trioxide (MoO_3) and tungsten trioxide (WO_3) [7].

Rutile (TiO_2) can accommodate relatively large deviations from stoichiometry (TiO_x with $2.0 \geqslant x \geqslant 1.75$) by the crystallographic shear (CS) mechanism [4, 5]. The formation of the CS planes is effectively a two-step process which involves the ordering of oxygen vacancies on a crystallographic plane and then their elimination by a shear of the lattice; Bursill and Hyde [10] have given a detailed description of possible mechanisms for the nucleation, growth and aggregation of CS planes. The periodic ordering of the CS planes in non-stoichiometric TiO_2 gives rise to a homologous series of phases with triclinic symmetry and with the general formula Ti_nO_{2n-1}, known as Magnéli or line phases. For $\sim 38 \geqslant n$ (even) $\geqslant 16$ ($1.97 \geqslant x \geqslant 1.94$) the CS planes are aligned parallel to $(1\,3\,2)_r$ [10, 15–17] (where r refers to the rutile subcell), and for $10 \geqslant n \geqslant 4$ ($1.90 \geqslant x \geqslant 1.75$) they are on $(1\,2\,1)_r$ [10, 18, 19]. For both types of CS planes the displacement vector is approximately $\frac{1}{2}[0\,\bar{1}\,1]_r$ [19, 20], and has been determined accurately for $(1\,3\,2)_r$ shear as $\frac{1}{2}\,[0, \overline{0.9}, 0.9]_r$ [20]. Fig. 1 shows schematically $\frac{1}{2}$ a $[0\,\bar{1}\,1]_r$ $(1\,2\,1)_r$ crystallographic shear in relation to the unit cell of rutile.

In the intermediate composition range, $16 > n > 10$ ($1.94 > x > 1.90$), the CS planes rotate cooperatively from between $(1\,3\,2)_r$ and $(1\,2\,1)_r$ [21, 22]. The change of CS plane from $(1\,2\,1)_r$ to $(1\,3\,2)_r$ has been described as an ordered intergrowth and uniform mixing of $(1\,2\,1)_r$ CS and $(0\,1\,1)_r$ anti-phase boundaries (APB) [21, 22] and is referred to as "swinging" shear.

Twins are a common microstructural feature in non-stoichiometric TiO_2 and are intimately related to the formation of shear structures [9, 10, 15]. These growth or translation twins form a boundary between regions which have sheared on equivalent but non-parallel planes of the original rutile structure. A TEM study of phases with $10 \geqslant n \geqslant 4$ found that the interface plane or composition plane of microtwins was parallel to $(1\,0\,0)_r$ in most cases and occasionally parallel to $(0\,1\,0)_r$ and $(0\,0\,1)_r$ [23]. For $n \leqslant 6$, however, no twinning was observed. Twinning of Ti_4O_7 has also been studied using both TEM and X-ray diffraction [23, 24], and the twins were found to be coherent, with boundaries on $(1\,0\,4)$ composition planes.

We report the results of a microstructural investigation of a hydrogen-reduced titania (TiO_2). The material studied was prepared with the objective of producing Ti_5O_9. Equilibrium conditions, however, are not

0022–2461/91 $03.00 + .12

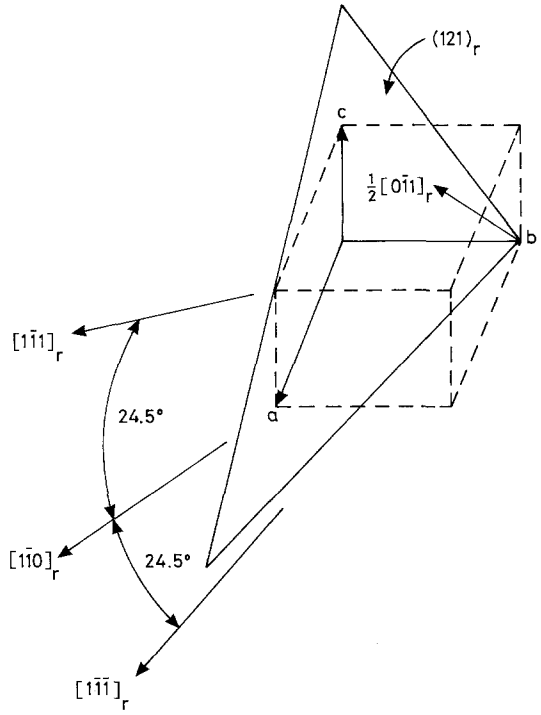

Figure 1 Schematic representation of $\frac{1}{2}a[0\bar{1}1]_r$ $(121)_r$ crystallographic shear in relation to unit cell of rutile.

achieved under flowing hydrogen and a range of line phases can form. It is the coexistence and distribution of these phases that we report here.

2. Materials and methods

A small block ($\sim 20 \times 10 \times 2\,mm^3$) of polycrystalline Ti_5O_9 was supplied by Imperial Chemical Industries (Runcorn, Cheshire, UK), who produce the material for use as electrochemical electrodes under the trade name "Ebonex". The starting powder was 99.5% purity titania with a grain size of $\sim 0.2\,\mu m$. The powder was mixed with a binder phase and plastically extruded into the required shape. The binder was then burnt off in air at $1\,°C\,min^{-1}$ to 500 °C. The material was reduced in flowing hydrogen at 1050 °C for 1 h, and then, after switching to argon, the temperature of the furnace was increased to 1250 °C and the material sintered for 1 h. The furnace was then switched off and the specimen cooled in argon over a period of 10 h.

TEM specimens were prepared from thin sections cut from close to the surface and from the centre of the original sample. These sections were ground and polished to a thickness of $\sim 30\,\mu m$ before mounting with epoxy resin onto copper grids. They were then ion beam thinned with argon ions accelerated at 5.5 kV. The specimens were then studied in a JEOL 2000-FX microscope operated at 200 kV and fitted with an X-ray microanalysis system with an energy dispersive spectrometer (EDS).

3. Results

3.1. Microstructure of Ti_5O_9

The microstructure of the TEM specimens prepared from close to the surface ($\sim 20\,\mu m$) and from the centre of the original specimen were similar, and for this reason all of the observations reported here, which were obtained from both types of specimen, are not distinguished. In terms of phase content this observation was confirmed by a serial X-ray diffraction

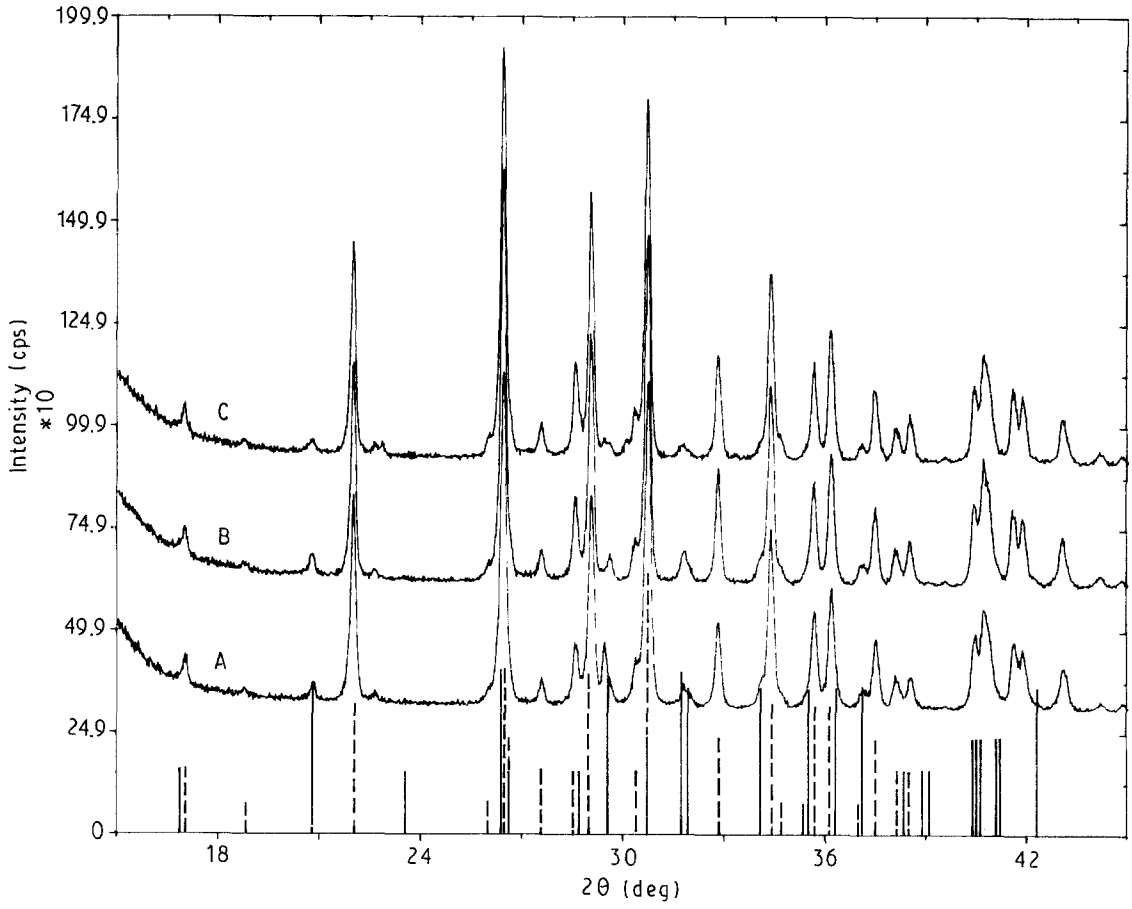

Figure 2 X-ray diffraction patterns recorded at a major surface of the original sample (A), 0.5 mm from the surface (B) and at the centre of the sample (C). (– – – Ti_5O_9, ——— Ti_4O_7)

analysis of the original sample. Fig. 2 shows the X-ray diffraction patterns for the surface (A), the centre (C) and an intermediate depth (B) of the original specimen parallel to its major face. The patterns are almost identical and show that Ti_5O_9 was the predominant phase and Ti_4O_7 a minor phase. X-ray diffraction patterns recorded from different parts of one of the major surfaces of the original bar of material showed that the composition of the bar was also homogeneous along its length. The molecular percentage of Ti_4O_7 in the material was estimated as 11% using the integrated intensities of the (1 0 2) peaks of the two phases and an equation described elsewhere [25].

The microstructure of the material was characterized by the presence of a large number of crystallographic twin boundaries, as shown in Fig. 3a (e.g. at A and B), and the individual grains often contained several parallel twins. The material had a grain size which varied between 1 and 10 μm and contained some porosity (C). The material was highly strained, as evinced by the presence of a high density of strain contours (Fig. 3a), and this made it very difficult to study the microstructure at low magnifications.

An amorphous second phase, formed by impurities in the material, was found at grain triple points (Fig. 3b) and contained silicon, calcium and a relatively small amount of aluminium (Fig. 3c).

Analysis of the electron diffraction patterns of individual grains from tilting experiments confirmed that the material consisted predominantly of Ti_5O_9. Fig. 4a shows a zone axis pattern parallel to the *b*-axis of Ti_5O_9, i.e. [0 1 0] (which is equivalent to $[1\,\bar{1}\,1]_r$ for the rutile subcell [10]).

In suitable crystallographic orientations, with the (0 0 1) planes (equivalent to $(1\,2\,1)_r$) parallel to the beam direction, it was possible to image the periodic spacing of the CS planes (Fig. 4b). These lattice fringe images showed that even when examined at high resolution relatively large areas within the grains (1×10^{-14} m^2) consisted of Ti_5O_9 phase with a perfect ordering of the spacings of the CS planes.

The crystallographic orientation of the twin boundaries was determined from electron diffraction patterns as (1 0 2), which is equivalent to $(0\,1\,1)_r$. Fig. 5a shows a diffraction pattern recorded at a twin boundary and with the twin plane parallel to the direction of the electron beam. It consists of two superimposed [0 1 0] zone axis patterns, which are related to each other by 180° rotation about the axis of the reciprocal lattice vector of (1 0 2), as illustrated diagramatically in Fig. 5b. Fig. 5c is a corresponding [0 1 0] zone axis lattice fringe image; it shows the (0 0 1) planes either side of the twin boundary meeting coherently. The orientation of the twin plane and the relative orientation of the (0 0 1) planes is not consistent with growth twinning associated with the formation of the CS structures; the angle between the (0 0 1) planes across the twin boundary (57°) is not consistent with any pair of the equivalent {1 2 1} planes. The twins, therefore, can only have formed by the twinning of the rutile subcell structure on $(0\,1\,1)_r$ planes.

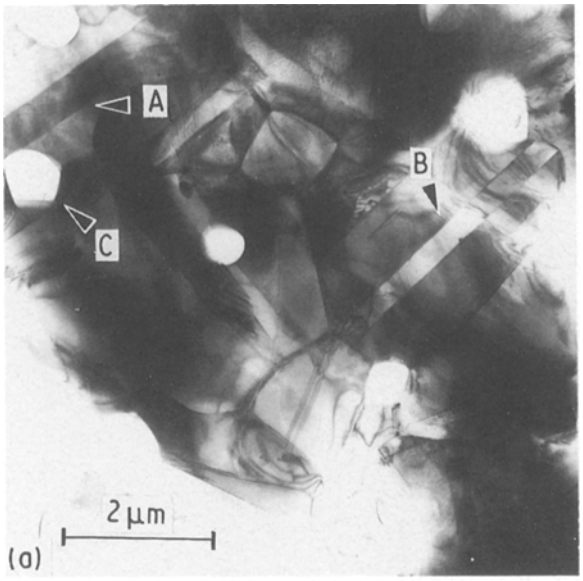

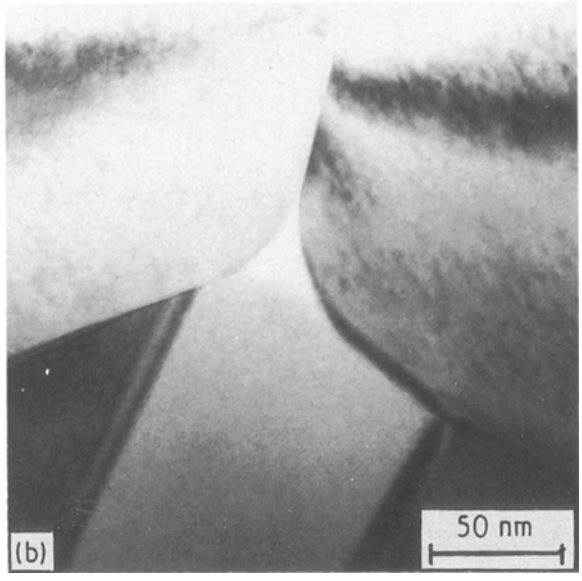

Figure 3 Microstructure of non-stoichiometric titania. (a) Low magnification image showing grain structure, twins (A and B) and porosity (C). (b) Grain triple point, with a twin band apparent in the lower grain. (c) EDS X-ray microanalysis spectrum of grain triple point shown in (b).

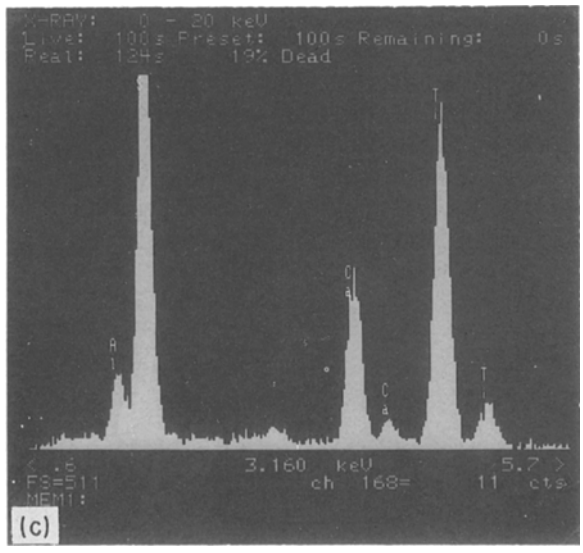

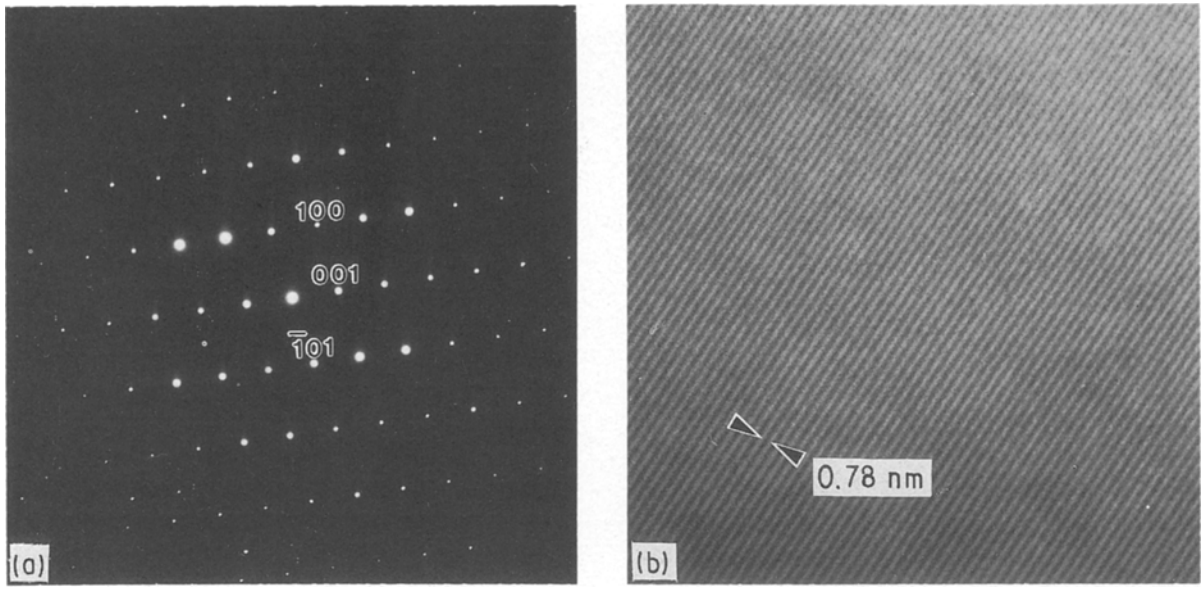

Figure 4 (a) [0 1 0] Zone axis electron diffraction pattern of Ti_5O_9. (b) (0 0 1) Lattice fringe image of Ti_5O_9.

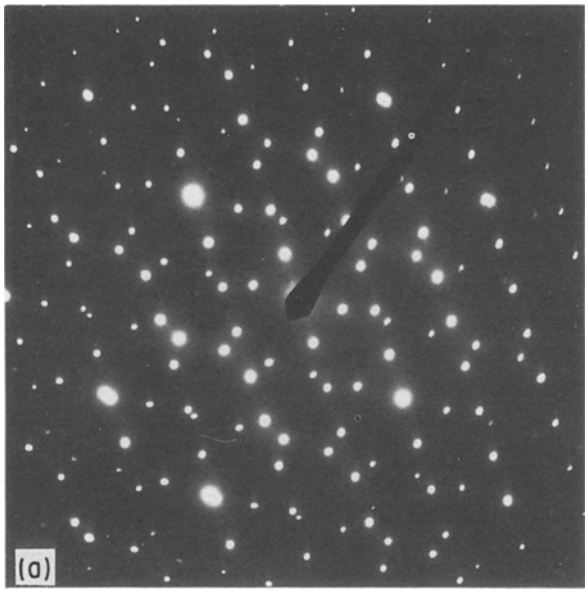

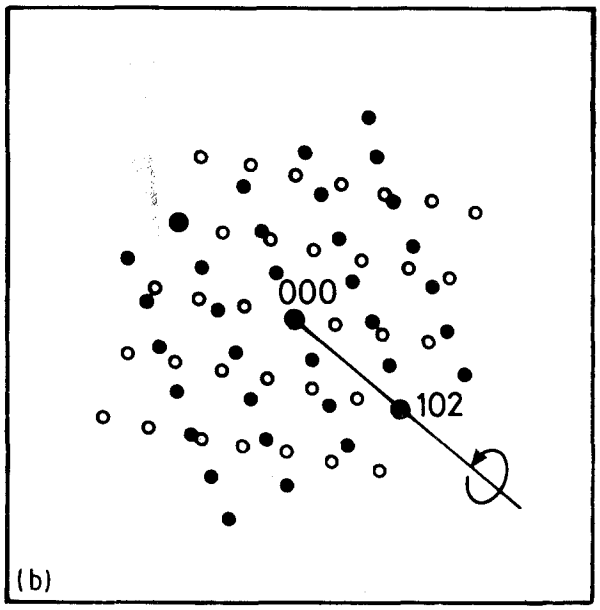

3.2. Second phases

For a high proportion of the grains examined weak second-phase reflections were also observed superimposed on the electron diffraction patterns of the Ti_5O_9 phase, and these were indexed as Ti_6O_{11}. In some cases, for small selected areas of grains, these reflections were relatively strong, as for example in Fig. 6a, which shows the overlapping 0 0 1 systematic rows for the two phases (the 0 0 1 reflections of the Ti_6O_{11} phase are marked). Lattice fringe images of (0 0 1) planes from these regions showed an epitaxial mixing of Ti_5O_9 and Ti_6O_{11} line phases on (0 0 1) planes (Fig. 6b). The Ti_6O_{11} phase usually formed

Figure 5 (a) Diffraction pattern recorded with direction of electron beam parallel to twin plane in Ti_5O_9 crystal. (b) Diagramatic representation of diffraction pattern. (c) (0 0 1) lattice fringe image of twin boundary recorded under the diffraction conditions shown in (a).

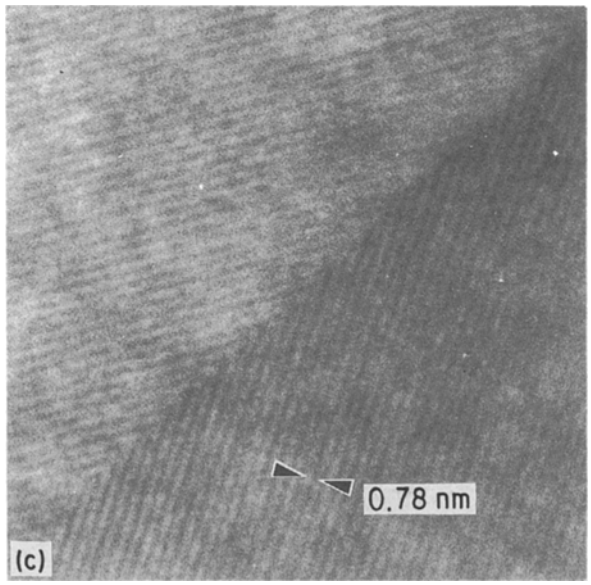

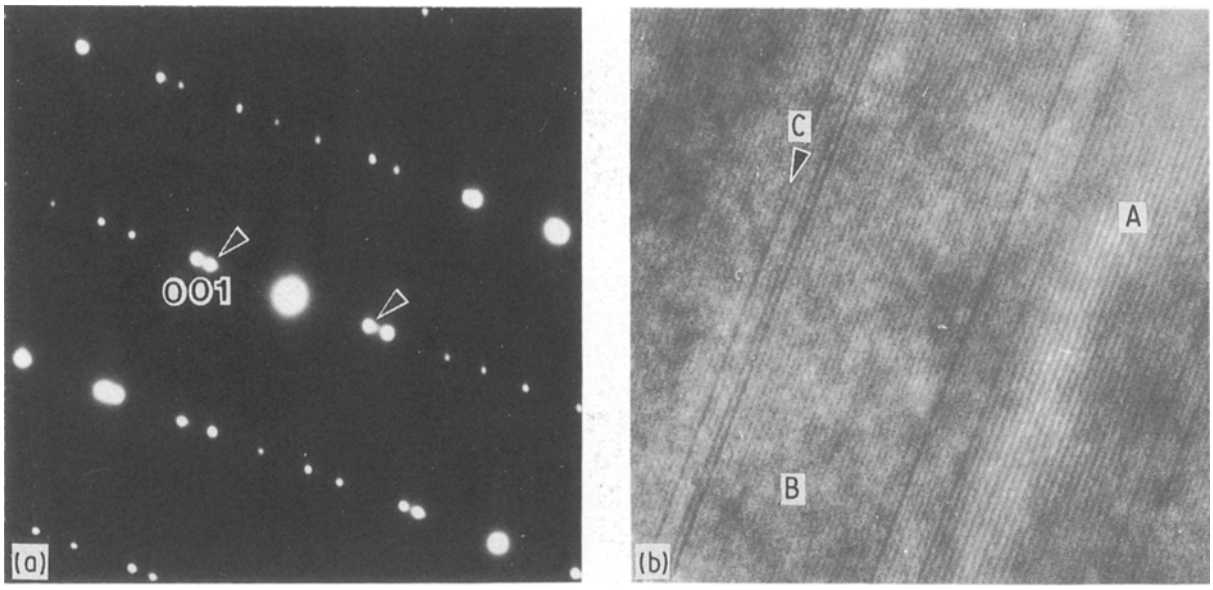

Figure 6 (a) Selected area diffraction pattern from part of a Ti_5O_9 grain containing second-phase reflections from Ti_6O_{11} (arrowed). (b) (0 0 1) lattice fringe image from same region (fringe spacing of Ti_5O_9 (B) is 0.78 nm and Ti_6O_{11} (A and C) is 0.95 nm).

long, narrow bands or lamellae (A) in the Ti_5O_9 phase (B) and sometimes consisted only of a single (0 0 1) planar spacing of 0.95 nm (C).

Of the many Ti_5O_9 grains studied using TEM ($\sim$ 30), the only second phase found in these grains was Ti_6O_{11}. It is surprising that Ti_4O_7 was not observed in the Ti_5O_9 grains as the X-ray diffraction results show that there must have been considerably more Ti_4O_7 present in the material than Ti_6O_{11} as Ti_6O_{11} was not even detected in the diffraction patterns (Fig. 2). It was only by methodically analysing the electron diffraction patterns of individual grains that Ti_4O_7 phase was eventually identified using TEM. When it was identified it was found to occur as single-phase grains. In the few grains we were able to identify as Ti_4O_7 we never observed second-phase reflections from other line phases in their diffraction patterns. Fig. 7a shows part of a twinned Ti_4O_7 grain.

The phase of several of the grains adjacent to the Ti_4O_7 grain shown in Fig. 7a was examined, and all of these grains were indexable as Ti_5O_9. The composition of the grains, including the Ti_4O_7 grain, was also analysed using X-ray microanalysis. None of the grains contained any detectable impurities, and only Ti was detected (oxygen is not detectable with the EDS system used).

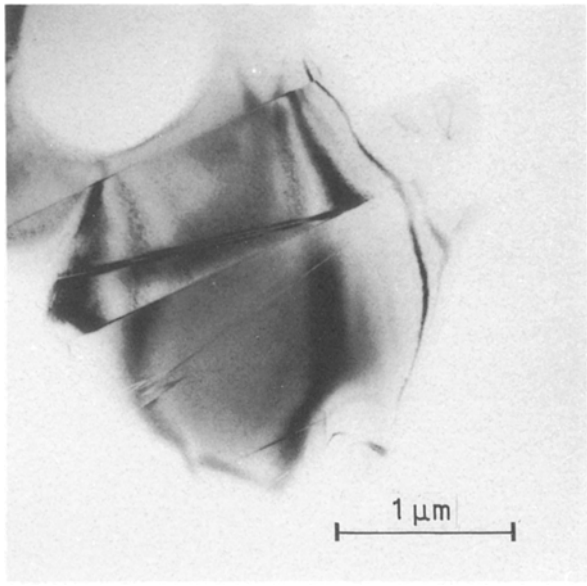

Figure 7 Part of twinned Ti_4O_7 grain.

3.3. Disposition of Ti_6O_{11} in Ti_5O_9

Although the Ti_6O_{11} phase usually occurred as narrow lamellae (< 10 nm wide) in the Ti_5O_9 phase, it was always easy to identify in diffraction contrast images because when the (0 0 1) epitaxial interfaces of the Ti_5O_9 and Ti_6O_{11} phases were tilted relative to the beam direction they produced stacking fault fringes. Overlap of the epitaxial layers and disorder in their spacing meant that the stacking fault fringe patterns were complex and clearly not formed by simple planar stacking faults (see A in Fig. 8a and the other faults parallel to it).

Fig. 8a and b shows corresponding bright field and dark field images of a region which contained a relatively high Ti_6O_{11} phase content. It shows a series of parallel twin boundaries which bound the twin bands labelled 1, 2, 3 and 4 in Fig. 8b. The images were obtained with the twin bands 1 and 3 under a two-beam condition and bands 2 and 4 with no strong diffraction condition, hence the strong contrast between the alternate twin bands. The faults which are parallel to those indicated at A and B were produced by lamellae of Ti_6O_{11} phase, and the region marked C is a much wider band of Ti_6O_{11}. The faults that are parallel to the twin boundaries are in fact microtwins (D, E and F).

The microtwins were almost as common as the

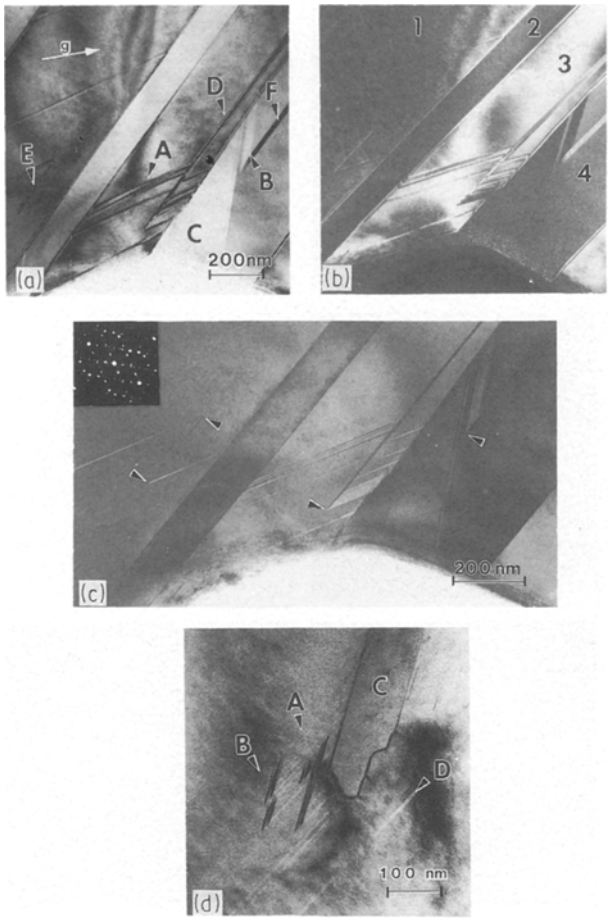

Figure 8 Region containing macrotwins, microtwins (D, E and F) and Ti_6O_{11} lamellae (A, B and C). (a) and (b) complimentary BF and DF images (twin bands 1 and 3 are under two-beam condition with $g = 1\,0\,\bar{1}$); (c) [0 1 0] Zone axis BF image. (d) BF image of Ti_6O_{11} lamellae (A) between microtwins (B) and macrotwin (C).

wider twin bands or, as we will now refer to them, the macrotwins. The width of the macrotwins was typically 0.1 to 1 μm, while that of the microtwins was at least an order of magnitude less, with widths of less than 10 nm. The microtwins were not only distinguished from the macrotwins by their distinctly narrower width but also by the fact that they were much more commonly seen to terminate (D and F) and were sometimes very short (E).

Fig. 8c is a bright field image of the same region in Fig. 8a but at a slightly higher magnification and recorded with the specimen orientated so that the twin and epitaxial phase boundaries were parallel to the beam direction, i.e., it is a [0 1 0] zone axis image. In this orientation the width and distribution of the microtwins and Ti_6O_{11} lamellae can clearly be seen. The second-phase reflections from the Ti_6O_{11} phase are recorded in the selected area diffraction pattern in the insert, and no other second-phase reflections are present.

It is clear from Fig. 8a, b and c that there was a strong interaction between the second-phase lamellae and the microtwins. This interaction is most apparent in Fig. 8c, in which it is noticeable that the tips of the terminating microtwins connect exactly with Ti_6O_{11} lamellae (see arrows); and this was a very common observation. Another good example of this is shown in Fig. 8d, where Ti_6O_{11} lamella (A) can be seen connecting with short microtwins (B). There is a macrotwin at C and part of a long Ti_6O_{11} lamellae at D which ran across the grain.

The second-phase lamellae were always discontinuous across the microtwins, suggesting that either the microtwins were formed before the second-phase lamellae or that the lamellae moved (which would have involved a reordering of the CS planes) subsequent to the formation of the microtwins.

Fig. 9a is a lattice fringe image of a region which showed several interesting microstructural features. The image was recorded with the electron beam parallel to the twin boundary plane and the (0 0 1) planes. A microtwin can be seen at A and a high density of Ti_6O_{11} lamellae at B. Region C corresponds to the termination or end of a twin band whose twinning plane is parallel to the trace of the boundary at D. The boundary between the two different twin orientations at E and F are faceted and have a preferred orientation. The plane on which the boundaries tended to align was parallel to the beam direction, as evinced by the narrowness of the boundary when viewed in this orientation. The trace of boundary at F corresponds closely to $(1\,0\,\bar{1})$ on side B of the boundary and $(2\,0\,\bar{5})$ on side F (these planes are equivalent to $(2\,1\,\bar{1})_r$ and $(1\,1\,0)_r$, respectively). The orientation of the boundary

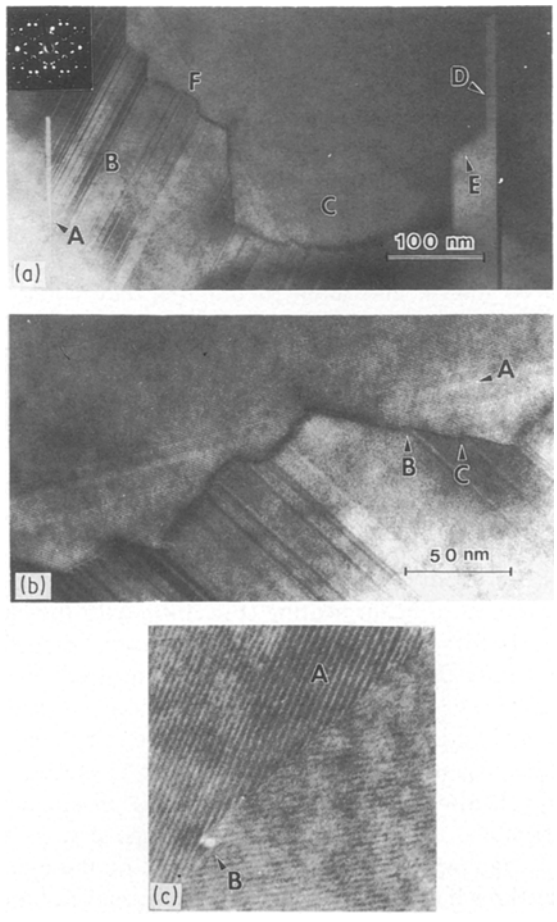

Figure 9 (a) Low magnification (0 0 1) lattice fringe image of terminating twin band (C) in region with Ti_6O_{11} lamellae (B) and microtwin (A). (b) Enlarged image of boundary near (F). (c) Ti_6O_{11} lamella (A) contacting twin boundary.

at E relative to the twinned regions is the reverse of that above.

The same preferred orientation was observed for individual twin boundary steps which were seen at the boundary of continuous twin bands. It was by means of these discrete steps (< 50 nm wide) that the width of continuous twin bands changed.

Fig. 9b shows the boundary near F at a higher magnification than Fig. 9a (the image has been rotated by ~ 90° anticlockwise). In the direction indicated by A a series of Ti_6O_{11} lamellae intersect the boundary and then continue on the other side of the intervening twin band. It is, therefore, apparent that the boundary and the Ti_6O_{11} phase have moved relative to each other at some stage. The Ti_6O_{11} lamellae would have probably been able to move more easily than the twin boundaries since their motion would have required only the rearrangement of Ti ions at the CS planes by diffusion, whereas the movement of $(0\,1\,1)_r$ twin boundaries would have required the rearrangement of the oxygen sublattice as well as diffusion of Ti ions.

We also noticed when examining twin boundaries at high magnification that very small steps at the boundary were quite common and that they were often associated with the presence of second-phase lamellae. In Fig. 9b at B and C steps at the twin boundary can be seen where two Ti_6O_{11} lamellae contact it. The same thing can be seen more clearly in Fig. 9c, which shows part of a narrow Ti_6O_{11} lamella at A (~ 15 nm wide) contacting a twin boundary near a small step (B). A similar observation was made by Yoshida *et al.* [26] when Ti_5O_9 and Ti_6O_{11} lamellae intersect a $(0\,1\,1)_r$ twin boundary in Ti_4O_7.

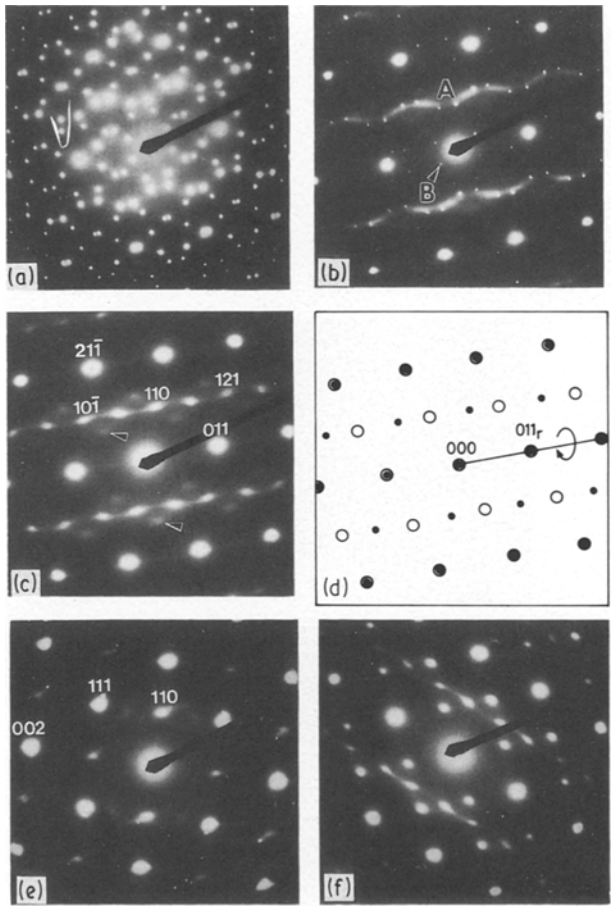

Figure 10 (a) Superimposed [0 1 0] zone axis diffraction patterns from adjacent twin bands; (b) Pattern after 10 minutes of beam heating. (c) After 15 minutes of beam heating pattern consists of two superimposed, twin related $[1\,\bar{1}\,1]_r$ zone axis patterns. (d) Diagramatic representation of diffraction pattern. (e) and (f) $[1\,\bar{1}\,0]_r$ and $[1\,\bar{1}\,\bar{1}]_r$ zone axis patterns, respectively, observed on tilting the specimen after the beam heating experiment was completed.

3.4. *In Situ* electron beam heating

During lattice imaging electron beam heating caused the lattice fringes to become irregular, wavy and difficult to image, and after 10 minutes they could no longer be imaged. In other imaging modes, which required a less intense beam, the effect of beam heating was usually not apparent. The structural alterations that occurred during beam heating were studied by using electron diffraction patterns recorded during an unsuccessful attempt to image lattice fringes at a twin boundary. The pattern in Fig. 10a, which shows two twin-related [0 1 0] zone axis patterns superimposed, was recorded before starting lattice imaging. After 10 minutes of beam heating (Fig. 10b), with the electron beam maximally converged (beam diameter ~ 0.5 μm), diffuse, "zagged" bands appeared in the patterns (A) and a number of reflections originally present had disappeared or become significantly weaker, e.g. (0 0 1) at B (Fig. 10b). After 15 minutes of beam heating further reflections had disappeared completely, including (0 0 1), while some new reflections had appeared (Fig. 10c). Some of these new reflections had evolved from the diffuse zagged bands seen in Fig. 10b. Beyond 15 minutes no further changes were seen in the diffraction patterns and the twin boundary was still apparent.

The diffraction pattern of the new phase was indexed as rutile, formed by *in situ* oxidation of Ti_5O_9 under beam heating (Fig. 10c). The pattern consists of two $[1\,\bar{1}\,1]_r$ zone axis patterns, which are rotated relative to each other by 180° about the axis of the reciprocal lattice vector of $(0\,1\,1)_r$ (Fig. 10d). The reflections of one of the twin orientation variants is labelled in Fig. 10c. Some faint reflections which could not be indexed are also present (arrowed), and these were probably produced by double diffraction effects. The specimen was also rotated about the axis of the $(1\,1\,0)_r$ plane and zone axis patterns of the rutile phase were found at 25° and 50° rotation relative to $[1\,\bar{1}\,1]_r$, and these were indexable as $[1\,\bar{1}\,0]_r$ and $[1\,\bar{1}\,\bar{1}]_r$ zone axes, respectively (Fig. 10e and f, and also see Fig. 1).

It is not possible to say what the localized temperature of the specimen was during beam heating, but *in situ* experiments in TEM by others suggest that temperatures of about 500 °C are attainable [27]. The atmosphere in the microscope column was 1×10^{-4} Pa, which would correspond to a P_{O_2} (atm) of the order of 10^{-9}. According to available phase equilibria data this would be sufficient to produce nearly stoichiometric TiO_2 ($x > 1.999$) even at 1000 °C, and, therefore, even greater oxidation at lower temperatures [7].

Fig. 11a to d shows the effect of beam heating on (0 0 1) lattice fringes. Fig. 11a shows a lamella of Ti_5O_9 (A) in a relatively large band of Ti_6O_{11} (B). The image was recorded about 2 minutes after starting imaging in this region, and the Ti_5O_9 planes were already distorted because of beam heating effects. The Ti_5O_9 lamellae terminates at a planar fault (C) which is parallel to the $(0\,1\,1)_r$ plane and which is either a microtwin or an anti-phase-boundary. After 5 minutes of beam heating the (0 0 1) planes of the Ti_5O_9 phase had almost disappeared, while those of the Ti_6O_{11} were still quite sharp (Fig. 11b). After 10 minutes the (0 0 1) planes of Ti_6O_{11} were highly distorted (Fig. 11c), and after 20 minutes had almost completely disappeared (Fig. 11d). In Fig. 11d $(1\,1\,0)_r$ lattice fringes (0.33 nm) are imaged, but are not well resolved.

It should be noted that as soon as the lattice fringes became distorted intermediate phases were forming prior to the formation of the rutile phase. These intermediate phases were highly disordered (Fig. 10b) and, therefore, did not correspond to the highly ordered higher oxide line phases that can form under slow, controlled oxidation conditions.

The rate of oxidation of the specimen would have been controlled by the diffusion of oxygen from its surface into the bulk. The fact that the (0 0 1) fringes for the Ti_5O_9 phase disappeared more quickly than those of the Ti_6O_{11} phase indicates that it has a higher oxygen diffusion rate. This observation is consistent with the available data on oxygen diffusion which shows that the diffusion coefficient for Ti_5O_9 is about a factor of 5 greater than that for Ti_6O_{11} [28].

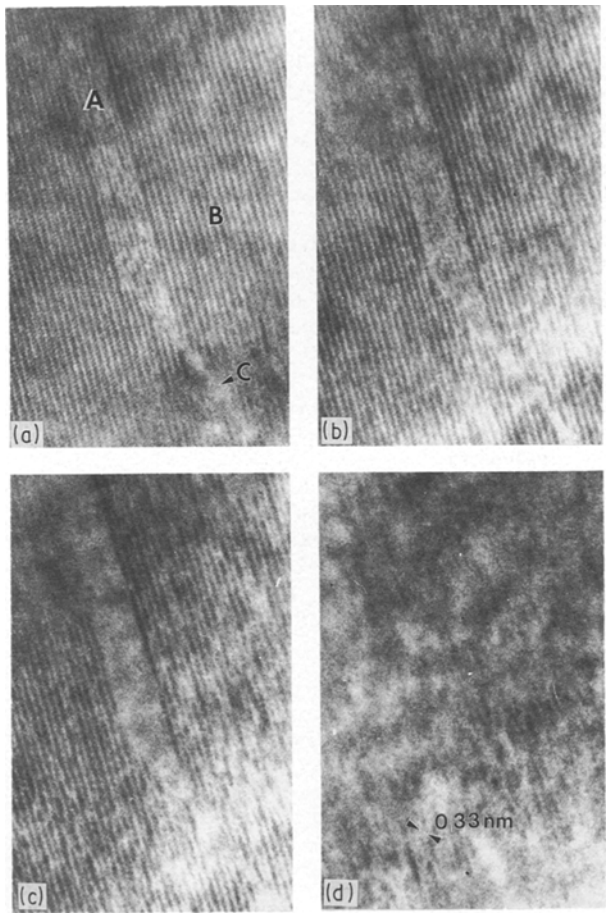

Figure 11 [0 1 0] Lattice image of Ti_5O_9 lamellae (A) inside relatively large region of Ti_6O_{11} after (a) 2 minutes, (b) 5 minutes, (c) 10 minutes and (d) 20 minutes of beam heating during imaging.

4. Discussion and conclusions

Our investigation of the microstructure of non-stoichiometric TiO_2 has revealed some interesting observations on the distribution and coexistence of line, or Magnéli, phases. We observed the phases Ti_4O_7, Ti_5O_9 and Ti_6O_{11}, of which Ti_5O_9 was the major phase. Although Ti_6O_{11} constituted only a very small percentage of the material (< 1 mol %) it was very conspicuous throughout the material because it formed narrow, epitaxial lamellae in Ti_5O_9 grains; local variations in the oxygen stoichiometry of the grains was simply accommodated by variations in the separation of the CS planes. In contrast, Ti_4O_7 phase seemed to occur as single-phase grains and was never observed as a second phase in Ti_5O_9 grains.

The distribution of the Ti_4O_7 as single-phase grains is surprising since we observed epitaxial mixing of the Ti_5O_9 and Ti_6O_{11} phases. We have no conclusive evidence to explain its heterogeneous distribution and can only speculate on how it might have occurred. A tentative explanation is that when the material was sintering gas was trapped in pores and that this micro-environment controlled the oxidation–reduction equilibria of the contacting grains, especially since diffusion of oxygen through the material would have been relatively slow.

The twins observed in previous studies of non-stoichiometric TiO_2 were predominantly growth twins which had been produced by the contact of domains in which shear had taken place on equivalent but non-parallel planes [9, 10, 23]. The twins we observed, however, were produced by twinning of the rutile subcell structure parallel to $(0\,1\,1)_r$, which is the common twinning plane for rutile [29]. The same twinning relation was observed by Yoshida *et al.* [26] in Ti_4O_7 and by Blanchin *et al.* [30] in slightly reduced TiO_2.

The fact that we did not observe growth twins associated with the formation of the crystallographic shear structures suggests that they were annealed out of the grains during reduction and sintering. The $(0\,1\,1)_r$ twins, however, would have been more difficult to anneal out because this would have involved a rearrangement of the oxygen sublattice, whereas movement of the growth twins would have required only diffusion of Ti ions. The difficulty in moving the $(0\,1\,1)_r$ twin boundaries was confirmed by the fact that during beam heating experiments we were unable to move them, even when the beam heating was intense enough to produce a phase change. *In situ* heating experiments performed by Blanchin *et al.* [30] indicate that temperatures of about 1000 °C are required to anneal out $(0\,1\,1)_r$ twins.

We observed that Ti_6O_{11} lamellae often ran across the width of a grain and were never seen to terminate within a grain, except when they contacted a twin boundary. Other authors have commented on their observation that CS structures were never seen to

terminate, and this they attributed to the high energy of the terminating dislocation [10]. The fact that we observed Ti_6O_{11} lamellae terminated and pinned at twin boundaries suggests that the twin boundary allowed a low energy configuration of the terminating CS planes that would have occurred because of the mismatch between Ti_5O_9 and Ti_6O_{11} structures.

Fig. 9c shows a Ti_6O_{11} lamella contacting a twin boundary in Ti_5O_9, and it is interesting to note that the (0 0 1) planes of Ti_6O_{11} seem to deviate near the boundary. Although caution has to be taken when interpreting lattice images, it is at least apparent that some structural alteration has taken place. It is well known that relaxation of the lattice occurs at CS planes because of electrostatic repulsion, particularly between the Ti ions, which form a double row at the CS plane [10]. The small distortion that this produces seems to be significant in accounting for the stability of the CS structures. It, therefore, seems possible that distortion of the lattice can also occur at twin boundaries, which would tend to reduce the boundary energy. These distortions would be particularly important when the boundary is incoherent, as could be the case when a Ti_6O_{11} lamella intersects a Ti_5O_9 twin boundary (Fig. 9c). They would help to make the boundary semicoherent, avoiding the need for dislocations (which would have a high energy), and could explain why the Ti_6O_{11} lamellae were pinned to the twins. It is interesting to note that $\{0\,1\,1\}_r$ is also the plane on which conservative anti-phase boundaries are commonly observed in non-stoichiometric TiO_2 [10, 20] and is the glide planes of rutile [10], which suggests it has a relatively low stacking fault energy.

The oxidation–reduction behaviour of non-stoichiometric TiO_2 is sluggish and shows a pronounced hysteresis [10, 31, 32]. This behaviour has been attributed to the difficulty of nucleating or eliminating CS planes and the presence of coherent boundaries, especially twin boundaries [10, 26, 31]. Our observations support the idea that twinning is a source for the hysteresis behaviour during oxidation–reduction and suggest that the presence of $\{0\,1\,1\}_r$ twins would make it very difficult to obtain single-phase material even under equilibrium conditions.

Acknowledgements

We thank K. Kendall and S. Tan for supplying us with material and for useful discussions regarding its fabrication.

References

1. A. D. WADSLEY, *Rev. Pure Appl. Chem.* **5** (1955) 165.
2. A. MAGNELI, *Acta Crystallogr.* **6** (1963) 495.
3. P. GADO, *ibid.* **A16** (1963) 182.
4. A. D. WADSLEY, "Nonstoichiometric Compounds", edited by L. Mandelcorn (Academic, London, 1964) p. 98.
5. A. D. WADSLEY, *Helv. Chem. Acta*, Werner Centenary Volume (1967) 208.
6. J. S. ANDERSON, *J. Chemical Society Dalton Transactions* (1973) 1107.
7. O. T. SORENSEN (ed), "Nonstoichiometric Oxides" (Academic, New York, 1981).
8. S. AMELINCKX and J. van LANDUYT, "The Chemistry of Extended Defects in Non-Metallic Solids", edited by L. Eyring and M. O'Keefe (North-Holland, Amsterdam, 1970) p. 295.
9. B. G. HYDE and L. A. BURSILL, *ibid.* p. 347.
10. L. A. BURSILL and B. G. HYDE, "Progress in Solid State Chemistry", Vol. 7, edited by M. Reiss and J. O. McCaldin (Pergamon, Oxford, 1972) p. 177.
11. J. S. ANDERSON, "Defects and Transport in Oxides", edited by M. S. Seltzer and R. I. Jaffee (Plenum, New York, 1974) pp. 25, 260.
12. J. M. COWLEY and S. IIJIMA, "Defects and Transport in Oxides", edited by M. S. Seltzer and R. I. Jaffee (Plenum, New York, 1974) p. 205.
13. J. S. ANDERSON, *J. Phys. (Paris)* **38** (1977) 17.
14. L. EYRING, "Nonstoichiometric Oxides", edited by O. T. Sorensen (Academic, New York, 1981) p. 337.
15. L. A. BURSILL, B. G. HYDE, O. TERASAKI and D. WATANABE, *Phil. Mag.* **20** (1969) 347.
16. L. A. BURSILL and B. G. HYDE, *ibid.* **23** (1970) 3.
17. *Idem., Acta Crystallogr.* **B27** (1971) 210.
18. S. ANDERSON and L. JAHNBERG, *Ark. Kemi.* **21** (1963) 413.
19. S. ANDERSON, *Acta Scand.* **14** (1960) 1161.
20. L. A. BURSILL and B. G. HYDE, *Proc. R. Soc. London* **A320** (1970) 147.
21. L. A. BURSILL, B. G. HYDE and D. K. PHILP, *Phil. Mag.* **23** (1971) 1501.
22. L. A. BURSILL, "Solid State Chemistry", edited by R. S. Roth and S. J. Schneider (Special Publication 364) (National Bureau of Standards, Washington, 1971) p. 727.
23. O. TERASAKI and D. WATANABE, *Jpn J. Appl. Phys.* **10** (1971) 292.
24. J. L. HODEAU, M. MAREZIO, C. SCHLENKER, R. BUDER and S. LAKKIS, *J. Appl. Crystallogr.* **9** (1976) 391.
25. D. GOLDSCHMIDT and M. WATANABE, *Mater. Res. Bull.* **20** (1985) 65.
26. K. YOSHIDA, Y. YAMADA, H. OTA, L. A. BURSILL and G. J. WOOD, *Phil. Mag.* **A44** (1981) 73.
27. G. van TENDELOO, H. W. ZANDBERGEN and S. AMELINCKX, *Solid State Commun.* **63** (1987) 389.
28. A. N. BAGSHAW and B. G. HYDE, *J. Phys. Chem. Solids* **37** (1976) 835.
29. C. PALACHE, H. BERMAN and C. FRONDEL, "Dana's System of Mineralogy", Vol. 1, 7th Edn (Wiley, New York, 1944) p. 555.
30. M. G. BLANCHIN, L. A. BURSILL, J. L. HUTCHINSON and P. L. GAI, *J. Phys. (Paris)* **C3** (1981) 95.
31. G. J. WOOD and L. A. BURSILL, *Proc. R. Soc. London* **A375** (1981) 105.
32. R. R. MERRITT, B. G. HYDE, L. A. BURSILL and D. K. PHILP, *Phil. Trans. R. Soc.* **A274** (1973) 627.

Received 5 June 1990
and accepted 31 January 1991